Time dependent hydraulic falls and trapped waves over submerged obstructions

C. Page[1] and E.I.Părău[2, a)]

[1)] *School of Computing Sciences, University of East Anglia, Norwich NR4 7TJ, UK*

[2)] *School of Mathematics, University of East Anglia, Norwich NR4 7TJ, UK*

We consider the classical problem of a free surface flowing past one or more disturbances in a channel. The fluid is assumed to be inviscid and incompressible, and the flow, irrotational. Both the effects of gravity and surface tension are considered. The stability of critical flow steady solutions, which have subcritical flow upstream of the disturbance and supercritical flow downstream, is investigated. We compute the initial steady solution using boundary integral equation techniques based on Cauchy integral formula, and advance the solution forward in time using a mixed Euler-Lagrange method along with Adams-Bashforth-Moulton scheme. Both gravity and gravity-capillary critical flow solutions are found to be stable. The stability of solutions with a train of waves trapped between two disturbances is also investigated in the pure gravity and gravity-capillary cases.

Keywords: free surface flows; hydraulic falls; gravity-capillary waves

[a)] Electronic mail: e.parau@uea.ac.uk

I. INTRODUCTION

Two-dimensional free surface flows past a disturbance in a channel, usually in the form of either a locally applied pressure distribution on the free surface or a submerged obstruction on the bottom of the channel, is a widely studied problem in fluid mechanics. Both steady and unsteady solutions have been investigated using fully nonlinear methods in the pure gravity, where the effects of surface tension are ignored, and the gravity-capillary cases.

The key parameters in describing the flow are the upstream and downstream Froude numbers

$$F_{up} = \frac{V}{\sqrt{gh}}, \qquad F = \frac{U}{\sqrt{gH}} = \left(\frac{h}{H}\right)^{\frac{3}{2}} F_{up}, \tag{1}$$

respectively, the downstream Bond number

$$\tau = \frac{\sigma}{\rho g H^2}, \tag{2}$$

and the shape of the disturbance. Here V and U are the respective steady flow velocities upstream and downstream of the disturbance, h and H are the upstream and downstream fluid depths respectively, g is the acceleration due to gravity, ρ is the fluid density, and σ is the coefficient of surface tension.

Most previous studies have concentrated on the case of a uniform flow where the mean depth of the fluid is the same up and downstream, i.e. $U = V$, $h = H$. The free surface then takes the form of either a solitary wave (e.g. see Vanden-Broeck[1] in the steady case, and Grimshaw, Maleewong and Asavanant[2], and Grimshaw and Maleewong[3] in the unsteady case), or has a periodic wave train downstream of the disturbance (e.g. see Grandison and Vanden-Broeck[4] in the steady case, Grimshaw and Maleewong[3] in the unsteady case).

Fewer studies have considered conjugate flow solutions. Steady hydraulic falls, where the flow upstream is subcritical ($F_{up} < 1$) and the flow downstream is supercritical ($F > 1$), resulting in the depth of the flow decreasing over the disturbance, past a single submerged obstruction were considered in the pure gravity case by Forbes[5]. Dias and Vanden-Broeck[6] later computed generalized hydraulic falls where a train of gravity waves exists upstream of the fall. However, these solutions are unphysical, as they violate the radiation condition. By including a second obstruction further upstream, Dias and Vanden-Broeck[7] found solutions with a train of waves trapped between the submerged obstructions. They were then able to

show that the generalized hydraulic fall solutions are physically relevant when considered as the localised flow over an obstacle in a flow configuration which includes at least one additional disturbance further upstream. These trapped wave solutions have also been observed experimentally, see Pratt[8]. When the additional obstacle is placed downstream, where the flow is supercritical, it has been shown that a solitary type wave is found over the additional obstruction, see Belward[9].

Fully nonlinear hydraulic fall solutions in the steady gravity-capillary case have been computed by Page, Grandison and Părău[10]. They showed that in order to obtain trapped wave solutions when capillary effects are included, unless the surface tension is very weak, the additional obstacle must be placed downstream. In this case, the trapped wave train occurs in the supercritical regime. Otherwise, placing an additional obstacle upstream results in solitary like waves appearing over the obstacle.

We are interested in the stability of the pure gravity and the gravity-capillary hydraulic fall solutions in both the one and two obstruction configurations. There is a small amount of existing literature examining the stability of the pure gravity hydraulic fall using a weakly nonlinear analysis. Chardard *et al.*[11] showed that the forced Korteweg-de Vries (fKdV) equation suggests that the hydraulic fall generated over a moving obstruction, in a fluid otherwise at rest, is stable. However, they noted that there is a problem in concluding the stability of 'rising fronts', where the Froude number is supercritical upstream and subcritical downstream, due to the complexity of the boundary conditions in this case.

The stability of the pure gravity hydraulic fall is also supported by the work of Donahue and Shen[12]. Using a fKdV equation, they perturbed an initial stationary hydraulic fall solution with white noise. It was demonstrated that as time evolves the white noise dissipates, and the solution returns to the shape of the initial hydraulic fall. They simulated the effect of the upstream discontinuity and showed that, provided the domain was large enough, the discontinuity did not locally affect the results.

In this paper we investigate the stability of the pure gravity and gravity-capillary hydraulic falls using the fully nonlinear equations. Chardard *et al.*[11] extended their stability analysis to pure gravity free surface profiles over two obstructions, and predicted that the generalized hydraulic fall is unstable. We extend the work in this paper to consider the stability of the trapped wave solutions found by Dias and Vanden-Broeck[7] and Page *et al.*[10].

In section II we formulate the problem mathematically using the unsteady fully nonlinear

equations. Then in section III we discuss the fully nonlinear scheme used to solve the problem numerically, and advance the solution forward in time. Our results are presented in section IV, and we finish with a conclusion and discussion of our findings in section V.

II. FORMULATION

We consider an incompressible, inviscid two-dimensional fluid, lying at rest in a channel. On the bottom of the channel, one or more arbitrarily shaped submerged obstructions move to the left with speed U. Cartesian coordinates (x^*, y^*) are introduced, such that the x^*-axis is aligned parallel to the undisturbed channel bottom, and the y^*-axis points vertically upwards, through an obstacle at time $t = 0$. The flow is assumed to be irrotational, and is subject to gravitational acceleration g in the negative y^*-direction.

Physically, when a submerged obstruction moves through a fluid at rest, one would require that as $x^* \to \pm\infty$ any disturbances should decay to zero. However, we seek hydraulic fall solutions which require that locally the depth of the fluid is different far upstream and downstream of the obstruction. Upstream the fluid has constant depth h and constant velocity $V - U$, and downstream constant depth $H < h$ and zero velocity. In order to overcome this problem we consider the work of Donahue and Shen[12]. Using a fKdV equation and a domain of size $-W < x^* < W$, they let their stationary hydraulic fall solution lie in the range $-W/2 < x^* < W/2$. Then, in order to satisfy the physical boundary condition that the flow is uniform and at rest as $x^* \to \pm\infty$, a jump must occur somewhere further up or downstream in the flow. This jump must occur at $\pm W/2$. Donahue and Shen simulated the consequential discontinuity created at the jump and found that this led to a disturbance propagating in both directions. However, provided that W is large enough, they showed that this disturbance can be ignored when considering just the flow in the local vicinity of the obstruction. We can therefore take $W/2$ to be infinitely long, and assume that the additional jump and discontinuities start at $x^* = -\infty$. At infinity we can then impose the hydraulic fall boundary conditions, and examine the flow just in the local vicinity of the obstacle. Physically, we could also choose to view the problem as a moving submerged obstacle pushing a bulk of fluid upstream (with speed $V - U$) in a fluid otherwise at rest.

We define the free surface and the channel bottom by $y^* = H + \eta^*(x^*, t^*)$ and $y^* = B^*(x^*, t^*)$ respectively, and non-dimensionalise the problem by taking H as unit depth, and

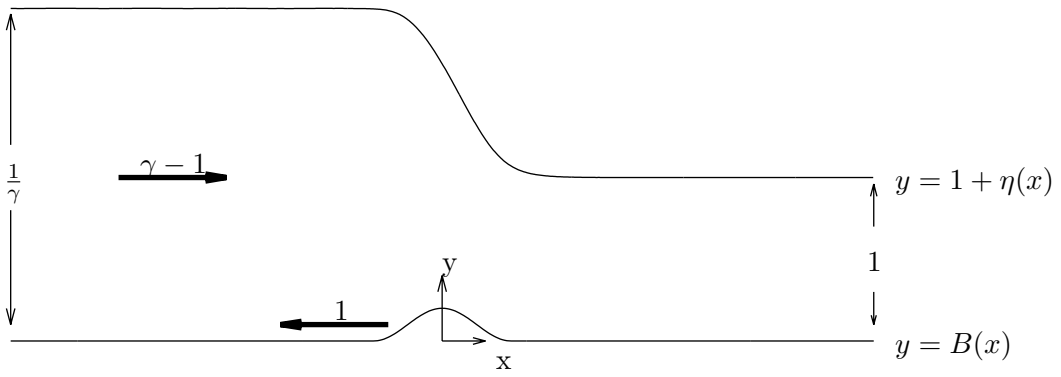

FIG. 1. Dimensionless local flow configuration over a single moving obstruction on the bottom of the channel.

U as unit speed. Non-starred variables are thus now understood to be dimensionless. The dimensionless upstream velocity is given by $(V - U)/U = \gamma - 1$, and thus, by conservation of mass, the dimensionless upstream depth is $1/\gamma$.

After introducing the velocity potential $\phi(x, y, t)$, the problem is formulated as a system of nonlinear equations. The Laplace equation

$$\nabla^2 \phi = 0 \tag{3}$$

must be satisfied in the fluid domain, subject to the free surface boundary conditions, and the kinematic boundary condition on the channel bottom

$$B_t + \phi_x B_x = \phi_y \quad \text{on } y = B(x, t). \tag{4}$$

To write the free surface conditions we follow the approach of previous work, for example Cooker *et al.*[13] and Grimshaw and Maleewong[2], which uses a mixed Euler-Lagrange method. We therefore write $(x, y) = (x, 1+\eta(x, t)) = (X(s, t), Y(s, t))$ on the free surface, where s is a parametrisation of the free surface. We also write $\phi(x, 1+\eta(x, t), t) := \phi(X(s, t), Y(s, t), t) := \Phi(s, t)$ on the free surface. The kinematic and dynamic conditions on the free surface are then expressed in Lagrangian form

$$\frac{DX}{Dt} = \frac{\partial \phi}{\partial x}, \tag{5}$$

$$\frac{DY}{Dt} = \frac{\partial \phi}{\partial y}, \tag{6}$$

$$F^2 \frac{D\phi}{Dt} = \frac{F^2}{2} \left(\left(\frac{\partial \phi}{\partial x} \right)^2 + \left(\frac{\partial \phi}{\partial y} \right)^2 \right) - y + \tau \kappa, \tag{7}$$

where $D/Dt = \partial/\partial t + \nabla\phi \cdot \nabla$ is the material derivative, and $\kappa = \eta_{xx}/(1+\eta_x^2)^{\frac{3}{2}}$ describes the curvature of the free surface.

Equations (5)-(7) then provide the means to advance a solution forward in time. To proceed, we write the partial derivatives ϕ_x and ϕ_y on the free surface as;

$$\phi_x = \frac{\phi_{\bar{s}} X_s - \phi_{\bar{n}} Y_s}{\sqrt{X_s^2 + Y_s^2}} \quad \text{and} \quad \phi_y = \frac{\phi_{\bar{s}} Y_s + \phi_{\bar{n}} X_s}{\sqrt{X_s^2 + Y_s^2}}, \tag{8}$$

where $\phi_{\bar{s}}$ and $\phi_{\bar{n}}$ are the derivatives in the tangential and normal directions respectively. Here, $\bar{s}$ denotes the arclength on the free surface, and we have used the relation

$$\phi_{\bar{s}} = \frac{\Phi_s}{\sqrt{X_s^2 + Y_s^2}}, \tag{9}$$

see for example, Dold[14]. Next, we scale the derivatives using

$$\phi_s = \phi_{\bar{s}} \sqrt{X_s^2 + Y_s^2}, \qquad \phi_n = \phi_{\bar{n}} \sqrt{X_s^2 + Y_s^2}, \tag{10}$$

where $\phi_s = \partial\Phi(s,t)/\partial s$. Then, denoting the derivatives with respect to s by a prime, we obtain

$$\phi_x = \frac{\phi_s X' - \phi_n Y'}{X'^2 + Y'^2} \quad \text{and} \quad \phi_y = \frac{\phi_s Y' + \phi_n X'}{X'^2 + Y'^2}. \tag{11}$$

As we seek hydraulic falls, the flow must be uniform in the far field, away from the obstructions. We therefore impose the conditions

$$\nabla\phi \to 0 \ \text{ as } \ x \to \infty, \tag{12}$$

$$\nabla\phi \to \gamma - 1 \ \text{ as } \ x \to -\infty. \tag{13}$$

This completes the formulation of the problem.

III. NUMERICAL SCHEME

To solve the system of nonlinear equations numerically, we employ the boundary integral scheme used by Cooker *et al.*[13], Grimshaw Maleewong and Asavanant[2] and Grimshaw and Maleewong[3].

At time $t = 0$, we begin by computing a steady fully nonlinear hydraulic fall solution using the scheme outlined in Page *et al.*[10] and Dias and Vanden-Broeck[7]. Here, the channel bottom is fixed, and the fluid flows past the obstacle from left to right. The unsteady

variables X, Y and ϕ_s on the free surface, at $t = 0$ and an initial guess for ϕ_x on the channel bottom are then obtained by considering the relationship between the variables in the steady and unsteady cases. By numerically integrating ϕ_s using the trapezoidal rule we obtain ϕ on the free surface at $t = 0$, and the variables B_x, X', X'', Y' and Y'' at $t = 0$ are obtained by numerical differentiation.

The remaining unknowns at $t = 0$ are ϕ_n on the free surface and ϕ_x on the channel bottom. They are obtained from two integral differential equations, see equations (16) and (17) below.

Firstly, we introduce the complex variable $z = x+iy$, and the complex potential $w(z,t) = \phi(x,y,t) + i\psi(x,y,t)$, where $\psi(x,y,t)$ is the stream function. The Cauchy integral formula is applied to the function

$$\chi = \frac{dw}{dz} = \phi_x - i\phi_y \tag{14}$$

around the contour $\mathcal{C}$, which consists of the free surface, the channel bottom, and lines joining them at $x = \pm\infty$. On the free surface we have

$$\chi = \frac{(\phi_s X' - \phi_n Y') - i(\phi_s Y' + \phi_n X')}{X'^2 + Y'^2}. \tag{15}$$

We take the evaluation point $z = X(s,t) + iY(s,t)$ to be on the free surface and let z^* be the varying point on the contour $\mathcal{C}$, such that $z^* = X(s^*,t) + iY(s^*,t) = X^* + iY^*$ on the free surface, and $z^* = x^* + iB(x^*) = x^* + iB^*$ on the channel bottom. Next, we multiply both sides of the Cauchy integral equation by $i(X' + iY')$, and then using the kinematic condition at a given time and taking the real part of the Cauchy integral formula, we obtain the integro differential equation

$$\begin{aligned}\phi_n(X(\xi),Y(\xi)) = &-\frac{1}{\pi}\int_{-\infty}^{\infty}\frac{\phi_s^*(X'(X^*-X)+Y'(Y^*-Y)) + \phi_n^*(Y'(X^*-X)-X'(Y^*-Y))}{(X^*-X)^2+(Y^*-Y)^2}ds^* \\ &+\frac{1}{\pi}\int_{-\infty}^{\infty}\frac{(\phi_x^*(1+B_x^{*2})+B_x^{*2})(X'(x^*-X)+Y'(B^*-Y)) + B_x^*(Y'(x^*-X)-X'(B^*-Y))}{((x^*-X)^2+(B^*-Y)^2)}dx^*.\end{aligned} \tag{16}$$

Similarly, when the evaluation point lies on the channel bottom $y = B(x,t)$, and we take the imaginary part of the equation, we obtain the second integro differential equation

$$\begin{aligned}\phi_x(x,B(x)) = &\frac{1}{\pi}\int_{-\infty}^{\infty}\frac{\phi_s^*(Y^*-B)+\phi_n^*(X^*-x)}{(X^*-x)^2+(Y^*-B)^2}ds^* \\ &-\frac{1}{\pi}\int_{-\infty}^{\infty}\frac{B_x^*(x^*-x)+(\phi_x^*(1+B_x^{*2})+B_x^{*2})(B^*-B)}{(x^*-x)^2+(B^*-B)^2}dx^*.\end{aligned} \tag{17}$$

The integro-differential equations (16) and (17) are solved numerically using Newton's method. The free surface and channel bottom are discretized using N and M equally spaced meshpoints, respectively. Thus, there are $N+M$ unknowns; $\phi_n(i)$ for $i=1,...,N$ and $\phi_x(i)$ for, $i=1,...,M$, where $\phi_n(i)$ represent the values of ϕ_n at grid point i on the free surface, and similarly for $\phi_x(i)$ on the channel bottom. The integro-differential equations are truncated at $-A$ and B, where A and B are large positive constants, and then evaluated at the $N+M-2$ mesh midpoints using the trapezoidal rule with summation over the meshpoints. Following Dias and Vanden-Broeck[15], the truncation error is minimized by considering the integrals from $-\infty$ to $-A$ and B to ∞. The integrals from B to ∞ approximate to zero, so can be neglected, but the integrals from $-\infty$ to $-A$ are non-zero. We evaluate them analytically by approximating the unknowns by their values at the first mesh point on the free surface and channel bottom respectively. We then obtain the corrections T_1 and T_2 to the truncated versions of the integro-differential equations (16) and (17), respectively;

$$\begin{aligned} T_1 =& -\frac{1}{2}\phi_s(1)X'(i)\log\left((X(1)-X(i))^2+(Y(1)-Y(i))^2\right) \\ & -\phi_s(1)Y'(i)\arctan\left(\frac{X(1)-X(i)}{Y(1)-Y(i)}\right) \\ & +\frac{1}{2}\phi_x(1)X'(i)\log\left((x(1)-X(i))^2+(B(1)-Y(i))^2\right) \\ & +\phi_x(1)Y'(i)\arctan\left(\frac{x(1)-X(i)}{B(1)-Y(i)}\right) \\ & -\frac{C}{2}(\gamma-1)Y'(i), \end{aligned} \tag{18}$$

where

$$C=\begin{cases} 0 & \text{if} \quad Y(1)<Y(i) \\ \pi & \text{if} \quad Y(1)=Y(i) \\ 2\pi & \text{if} \quad Y(1)>Y(i) \end{cases}, \tag{19}$$

and

$$\begin{aligned} T_2 =& \frac{\phi_s(1)}{X'(1)}\left(\arctan\left(\frac{X(1)-x(i)}{Y(1)-B(i)}\right)+\frac{\pi}{2}\right) \\ & -\phi_x(1)\left(\arctan\left(\frac{x(1)-x(i)}{B(1)-B(i)}\right)+\frac{D}{2}\right), \end{aligned} \tag{20}$$

where

$$D = \begin{cases} -\pi & \text{if} \quad B(1) < B(i) \\ 0 & \text{if} \quad B(1) = B(i) \\ \pi & \text{if} \quad B(1) > B(i) \end{cases}. \tag{21}$$

We now have $N-1$ equations from the first integral equation, together with its truncation correction T_1, and $M-1$ equations from the second integral equation, with its truncation correction T_2. The remaining two equations come from defining the flow in the far field, and are given by

$$\phi_x(1) = \gamma - 1 \quad \text{on} \quad y = B(x), \tag{22}$$

$$\phi_n(N) = 0 \quad \text{on} \quad y = 1 + \eta(x). \tag{23}$$

The equations (16), (17), (22) and (23) are then solved numerically at a given time, to find the $N+M$ unknowns, ϕ_n and ϕ_x, on the free surface and the channel bottom respectively.

Using equations (11) we obtain ϕ_x and ϕ_y on the free surface, and can thus march the solution forward in time using the fourth-order Adams-Bashforth-Moulton scheme to solve the equations (5)-(7). As this scheme requires information from the previous three time steps, we use the single step fourth order Runge-Kutta algorithm for the first three time steps from the initial steady solution.

We summarize the algorithm used to solve the problem as follows:

1. Obtain an initial steady solution using the scheme defined in Page *et al.*[10] or Dias and Vanden-Broeck[7]. Obtain the related unsteady variables, and initialize $\phi_n = \phi_x = 0$.

2. Approximate X', X'', Y', Y'', ϕ_s and their midpoints using finite differences and a four point dyadic interpolation scheme.

3. Solve the integro-differential equations (16) and (17) numerically using Newton's method, to find ϕ_n and ϕ_x on the free surface and channel bottom respectively. Then calculate ϕ_x and ϕ_y on the free surface by substituting the values found into (11).

4. Advance X, Y and ϕ forward in time on the free surface, using equations (5)-(7). Repeat from step two.

IV. RESULTS

In this section we present results obtained using the numerical method described in Section 3. Following Dias and Vanden-Broeck[7] and Page *et al.*[10], the submerged obstructions on the bottom of the channel are given cosine squared profiles of the form

$$B(x,t) = \begin{cases} 2A_1 \cos^2\left(\frac{\pi(x+x_d+t)}{2L_1}\right) & -L_1 < x + x_d + t < L_1, \\ 2A_2 \cos^2\left(\frac{\pi(x+t)}{2L_2}\right) & -L_2 < x + t < L_2, \\ 0 & \text{otherwise.} \end{cases} \tag{24}$$

The height and widths of the obstructions are thus defined by $2A_i$ and L_i, $i = 1, 2$ respectively. The obstacle with height A_2 has been chosen so that initially, at time $t = 0$, it is centered at the origin. At all time, the obstructions are separated by a distance x_d. In the case of solutions over a single obstruction, we set $A_1 = 0$.

In order to ensure the accuracy of our numerical scheme and to motivate the study of the stability of hydraulic falls, we first modifed our scheme to look for time dependent forced solitary waves. We removed the truncation corrections (18) and (20) and modified the far field conditions (22) so that there is no flow upstream as $x \to \pm\infty$;

$$\phi_x(1) = 0. \tag{25}$$

We describe in detail the solutions we obtained in such a configuration, in the appendix at the end of the paper. The solutions were in agreement with the results obtained in previous work by Grimshaw and Maleewong[3] and Chardard *et al.*[11]. Thus, they validate the numerical scheme in section III, which we now use to investigate the stability of hydraulic fall solutions.

A. Gravity hydraulic falls

Gravity hydraulic fall solutions which have subcritical flow ($F_{up} < 1$) upstream and supercritical flow ($F > 1$) downstream are examined. We therefore set $\tau = 0$, $A_1 = 0$, and take $A_2 > 0$ so that $y = B(x,t)$ describes a channel bottom with just a single moving obstruction.

In figure 2 we show the evolution of a hydraulic fall with $F = 1.34$, over an obstruction characterised by $A_2 = 0.05$, $L_2 = 3.2$. The hydraulic fall is seen to maintain its shape,

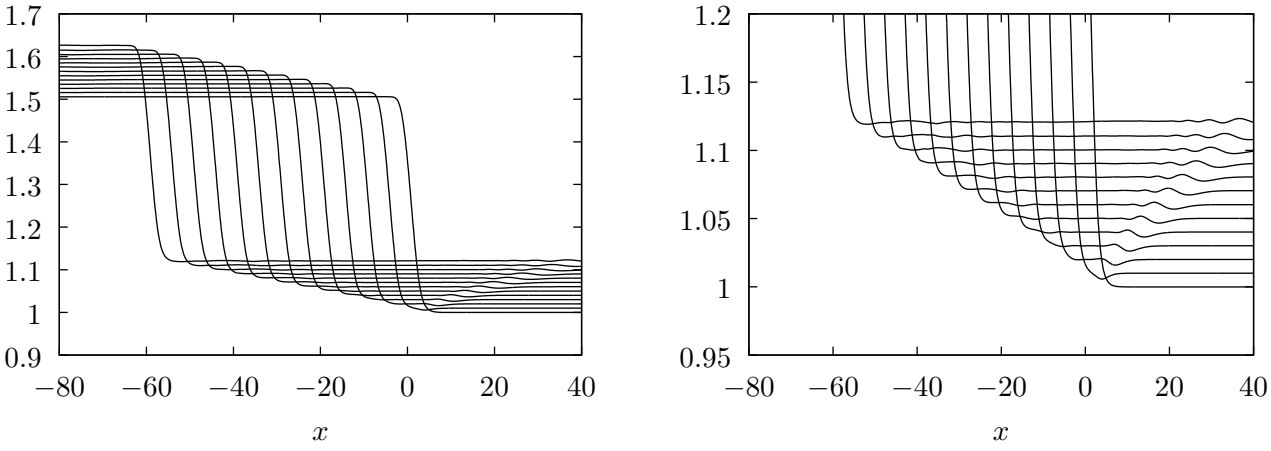

(a) (b)

FIG. 2. (a) Evolution in time of a pure gravity hydraulic fall profile with $F = 1.34$. Initially, a steady free surface profile is utilized (the lowest profile). The vertical axis is then moved upwards by 0.01 for each plot shown, such that $t_n = 5n$ for plots $n = 0, ..., 12$. (b) A close-up of the downstream free surface evolution shown in (a).

and moves upstream with the submerged obstruction. This suggests that the pure gravity hydraulic fall is stable. Downstream of the fall a small decaying wave train is generated and propagates downstream as time progresses. As time continues to evolve, further waves appear to be shed downstream of the fall. These waves propagate slowly upstream of the hydraulic fall. The evolution of the downstream profiles can be seen in figure 2(b). It is likely that these waves are the result of implicitly perturbing the solution at $t = 0$, by using the numerical methods involved in the scheme outlined in section III to approximate the initial solution.

Next we add a perturbation to the initial steady flow over the fall, of the form

$$y = y_s(1 + \lambda \cos(\mu x) e^{-\left(\frac{x}{2}\right)^2}) \tag{26}$$

where $\lambda \leq 0.1$ and $\mu \leq 10$ are positive constants, and y_s is the initial steady state solution. We find that as we advance the solution forward in time this perturbation decays, and the solution settles to the steady hydraulic fall solution. However, a small wave train is generated after the fall and propagates very slowly downstream. As we continue to advance the solution forward in time, a further wave train is shed from the bottom of the hydraulic fall and this propagates very slowly upstream. Figures 3 and 4 show the evolution of the

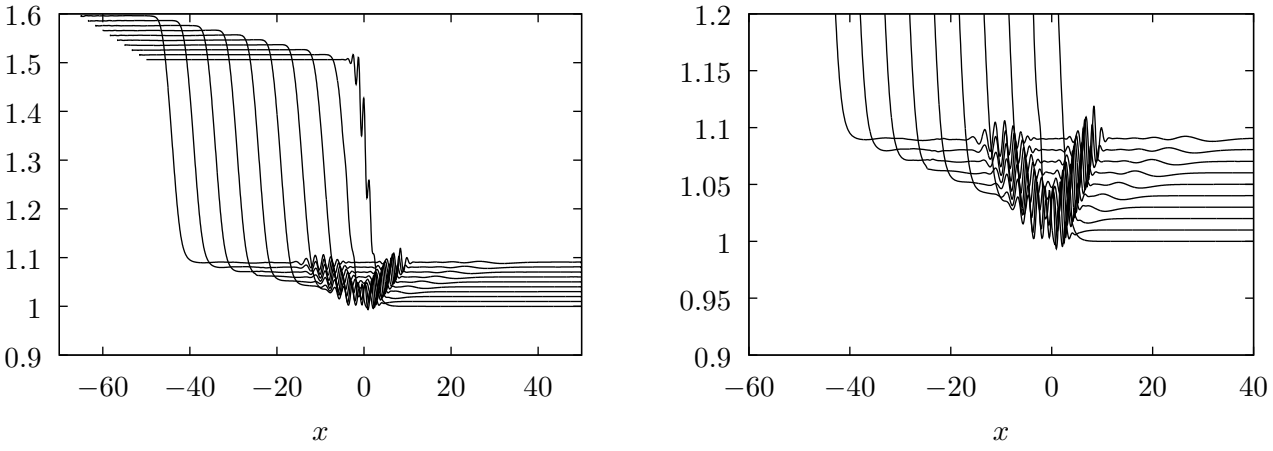

(a) (b)

FIG. 3. (a) Evolution in time, of a pure gravity hydraulic fall profile with $F = 1.35$. Initially, a steady free surface profile is perturbed (the lowest profile). The vertical axis is then moved upwards by 0.01 for each plot shown, such that $t_n = 5n$ for plots $n = 0, ..., 9$. (b) A close-up of the downstream free surface evolution shown in (a).

hydraulic fall with $F = 1.344$, over an obstruction classified by $A_2 = 0.05$, $L_2 = 3.2$. The propagation of the waves downstream of the hydraulic fall is clearly seen as time progresses. Locally, over the obstruction, figure 4(d) shows that the solution profile has become that of a classical hydraulic fall in the absence of a perturbation. Explicitly perturbing the solution has thus increased the disturbances shed from the hydraulic fall. However, all our results suggest that the pure gravity classical hydraulic fall is stable, and are thus in agreement with those obtained by Chardard *et al.*[11] and Donahue and Shen[12] using a weakly nonlinear analysis.

B. Gravity trapped waves

When $A_1 \neq 0$ and the second obstruction is placed upstream of the hydraulic fall ($x_d > 0$), Dias and Vanden-Broeck[7] have shown that a train of gravity waves may be found, trapped between the two obstructions. We follow this solution in time and observe that, as time evolves, the wavelength and amplitude of the waves appears to remain constant, see for example, the solution profile shown in figure 5. The persistence of the shape of the free surface suggests that the trapped wave solutions are also stable. Such solutions have also

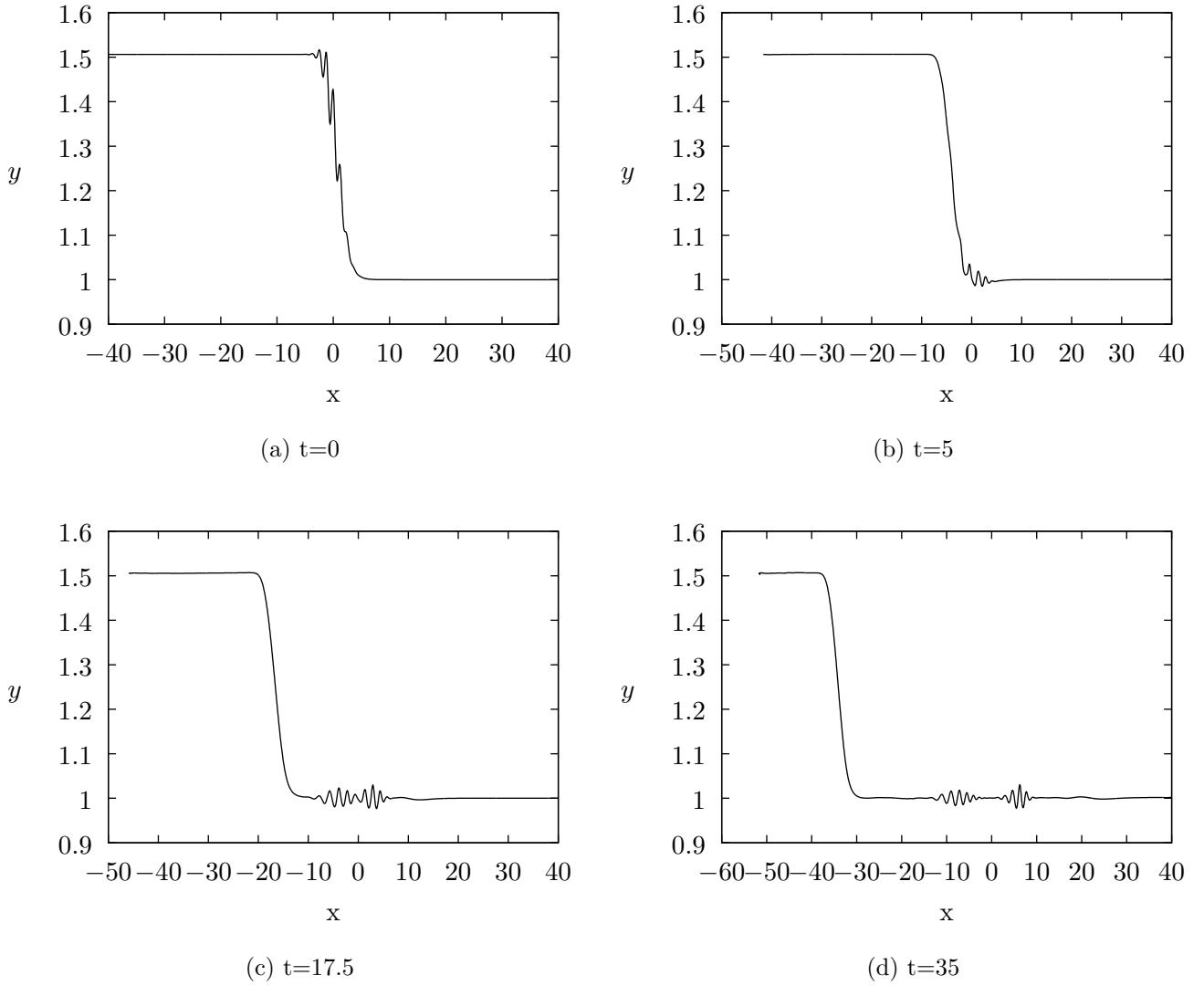

FIG. 4. Free surface profiles of the initially perturbed pure gravity hydraulic fall with $F = 1.35$, at different time steps; (a) $t = 0$, (b) $t = 5$, (c) $t = 17.5$, and (d) $t = 35$.

been observed in experiments. Pratt[8] choose the height and lengths of the submerged obstructions in his experiments for example, so that the flow would take the form of long waves. He was then able to interpret his results in terms of the weakly nonlinear Korteweg-de Vries model equation. He observed different types of steady solutions including hydraulic falls and the solutions obtained by Dias and Vanden-Broeck[7], with a train of waves trapped solely between the two obstacles. So the stability of the pure gravity hydraulic falls and trapped wave solutions appears to be a physically realistic result; we would indeed expect these solutions to be stable.

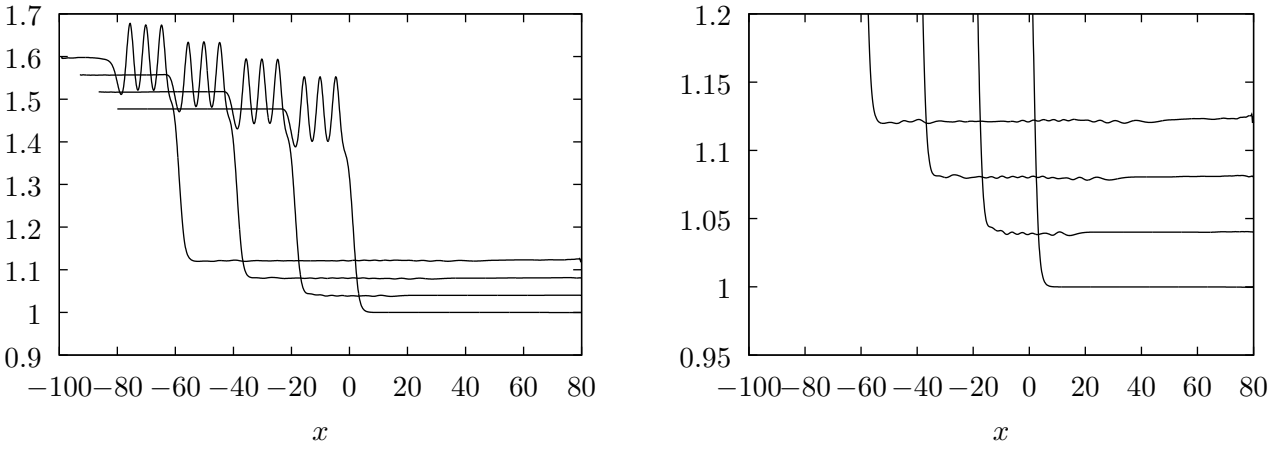

(a) (b)

FIG. 5. (a) Time evolution of a pure gravity hydraulic fall profile, $F = 1.33$, with a train of waves trapped between two obstructions. Initially, a steady free surface profile is utilized (the lowest profile). The vertical axis is then moved upwards by 0.04 for each plot shown, such that $t_n = 20n$ for plots $n = 0, ..., 3$. (b) A close-up of the downstream free surface evolution shown in (a).

Downstream of the hydraulic fall a small amplitude wave train is found. As time progresses the length of the flow domain which is effected by the downstream disturbances grows. The downstream part of the free surface profiles can be seen in figure 5(b). A second wave train is shed from the hydraulic fall as in the single obstruction results in the previous two sections. This second wave train propagates upstream with the hydraulic fall.

C. Gravity hydraulic falls with a solitary type wave

When $x_d < 0$, so that the second obstruction is found downstream of the hydraulic fall, in the steady case a solitary type wave is found to form over the additional obstruction, see Belward[9]. Following this solution in time we find that it is also stable. Both the hydraulic fall and the solitary type wave are found to move downstream with their respective obstacles. The solitary wave is a perturbation from the uniform stream. Such solutions have previously been shown to be stable, see for example the appendix. We have shown in section IV A that the hydraulic fall is stable and so one would expect the hybrid solution of the hydraulic fall followed by the solitary wave to be stable, as found.

Figure 6 shows the evolution of this type of solution with time. Downstream of the

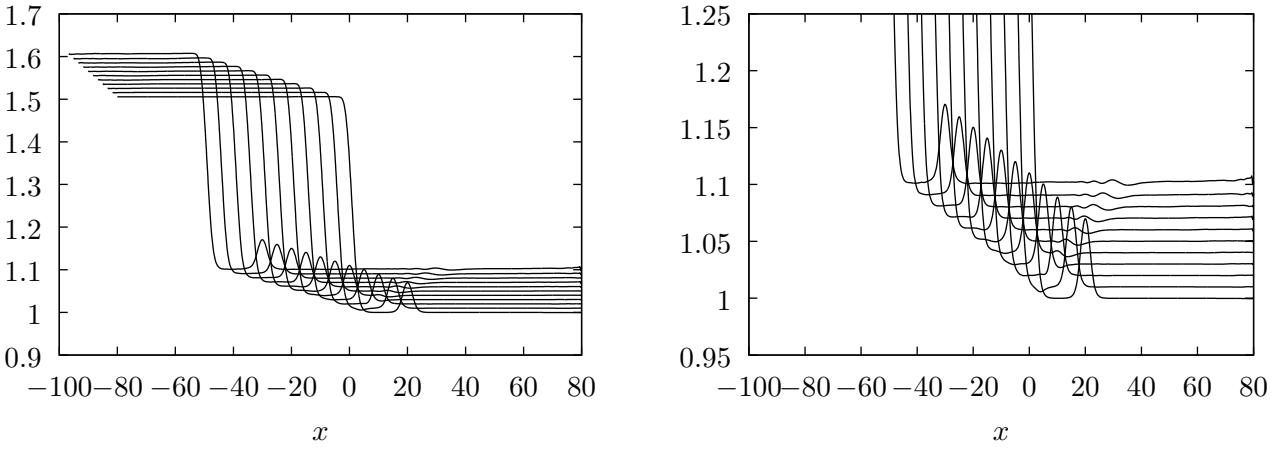

(a) (b)

FIG. 6. (a) Time evolution of a pure gravity hydraulic fall profile, $F = 1.35$, with a solitary type wave downstream of the fall. Initially, a steady free surface profile is utilized (the lowest profile). The vertical axis is then moved upwards by 0.01 for each plot shown, such that $t_n = 5n$ for plots $n = 0, ..., 10$. (b) A close-up of the downstream free surface evolution shown in (a).

hydraulic fall a small disturbance develops. The width of this disturbance grows slowly as it advances downstream past the solitary type wave.

D. Gravity-capillary hydraulic falls

Next, we include the effects of surface tension in our numerical scheme and consider results for different values of τ. Initially, we compute the gravity-capillary hydraulic fall solutions obtained in Page *et al.*[10]. Small amplitude numerical waves resulting from truncating the domain downstream at $A > 0$ instead of infinity, for some large constant A, appear downstream of the fall. We advance initial solutions, with different values of τ, forward in time. It is found that the hydraulic falls maintain their shape and move upstream with the submerged obstruction. As in the pure gravity case, a wave is shed from the fall and moves downstream away from the obstruction. Furthermore, we see that the numerical waves advance with the hydraulic fall so that far downstream, at greater time, the free surface appears to be uniform, in the absence of any disturbances shed from the hydraulic fall.

Figure 7(a) shows an advancing solution profile with $F = 1.36$, $\tau = 0.3$. It can be seen

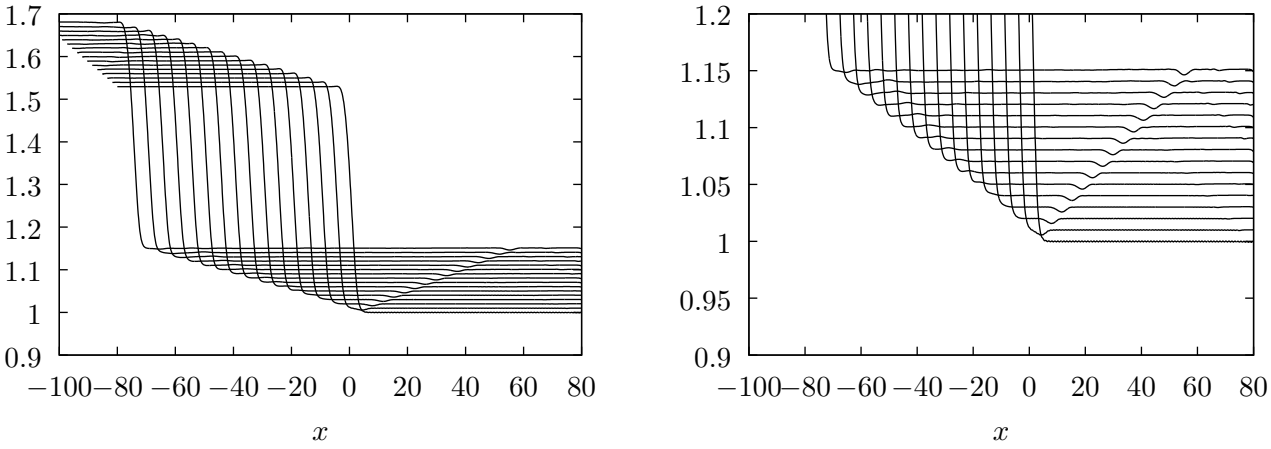

(a) (b)

FIG. 7. (a) Time evolution of gravity-capillary hydraulic fall profiles with $\tau = 0.3$. Initially, a steady free surface profile is utilized (the lowest profile). The vertical axis is then moved upwards by 0.01 for each plot shown, such that $t_n = 5n$, $n = 0, ..., 15$. (a) A close-up of the downstream free surface evolution shown in (b).

that firstly, a depression wave is shed from the fall, which propagates downstream. As time progresses an elevation wave then starts to emerge, propagating steadily upstream with the fall. Wave trains which are roughly symmetrical about $x = 0$ propagate both upstream and downstream of the fall, as time progresses, for the hydraulic fall with $F = 1.37$ and $\tau = 0.6$. In all the cases we considered, for $0.1 \leq \tau \leq 0.9$, locally, over the obstruction we found that the hydraulic fall maintained its shape as time evolved. This suggests that the gravity-capillary hydraulic fall is also stable.

When the surface tension is weak upstream, the upstream dispersion relation possesses a minimum. Page *et al.*[10] showed that as the upstream Froude number of the hydraulic fall solution is increased towards this minimum, a small decaying wavetrain appears on the free surface immediately before the hydraulic fall. Using such a solution profile at initial time, we follow this result in time. Figure 8 shows the time evolution of the free surface. As time develops, the upstream wave train does not appear to change form. The solution profile maintains its shape, suggesting that this solution is also stable.

We now add a perturbation in the form given by (26), to the initial steady solution. As the solution advances forward in time we see that this initial perturbation spreads out very

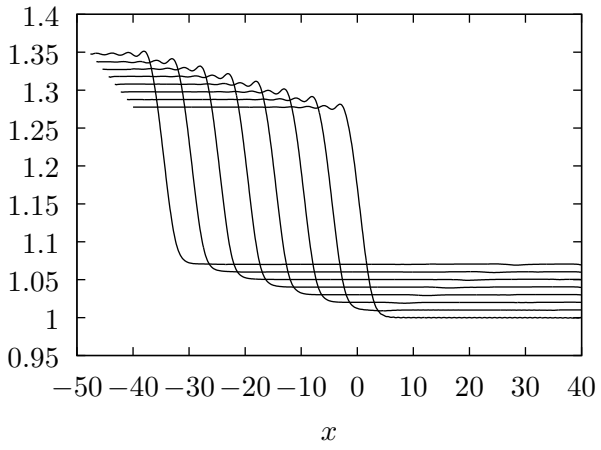

FIG. 8. Time evolution of a gravity-capillary hydraulic fall profile with $\tau = 0.2$, $F = 1.2$, past an obstruction characterised by $A_2 = 0.015$, $L_2 = 3.2$. Initially, a steady free surface profile is utilized (the lowest profile). The vertical axis is then moved upwards by 0.01 for each plot shown, such that $t_n = 5n$ for plots $n = 0, ..., 10$. A small decaying wave train can be seen upstream of the hydraulic fall.

quickly and radiates away so that the local solution, over the obstruction, settles to the classical gravity-capillary hydraulic fall. This supports the suggestion that including surface tension in the scheme, does not change the stability of the hydraulic fall.

Downstream of the hydraulic fall, waves continue to be shed, as in the pure gravity case. However, it appears that the capillarity dampens the waves; they are much less prominent in the gravity-capillary cases than in the pure gravity case. Figure 9 demonstrates this, showing two solution profiles, with $\tau = 0.1$ and $\tau = 0.6$.

E. Gravity-capillary trapped waves

Page *et al.*[10] obtained gravity-capillary solutions with a train of waves trapped between two obstructions. Unless the surface tension is very small, the second obstruction is placed downstream of the hydraulic fall. Following Page *et al.* we obtain a steady solution. Then, using this result as the initial profile for our numerical scheme, we follow the solution in time. A typical free surface profile with $\tau = 0.7$ is shown in figure 10. The trapped waves in this case appear to be unstable. In figure 10(b) we show the initial solution at time $t = 0$ (the solid line), superimposed with the solution at time $t = 14$ (the dashed line). It is clearly

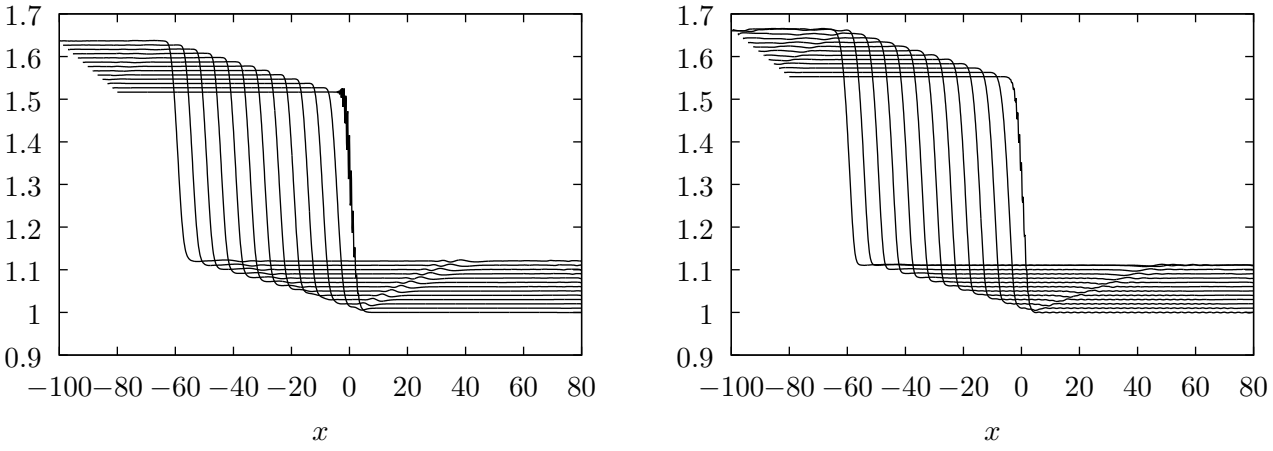

FIG. 9. Time evolution of gravity-capillary hydraulic fall profiles; (a) $\tau = 0.1$, (b) $\tau = 0.6$. Initially, a steady perturbed free surface profile is utilized (the lowest profile). The vertical axis is then moved upwards by 0.01 for each plot shown, such that $t_n = 5n$ for $n = 0, ..., 12$.

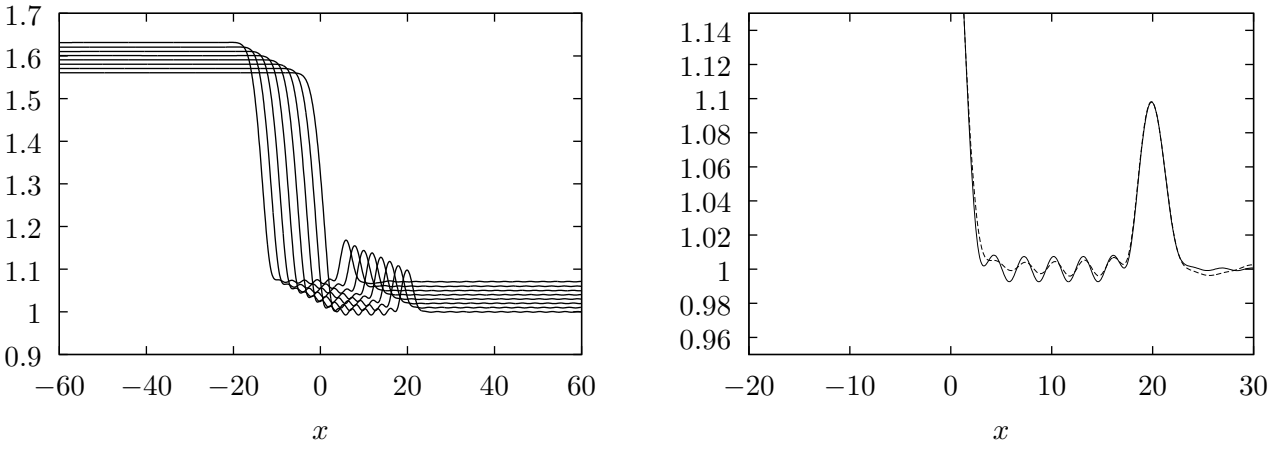

FIG. 10. Time evolution of a gravity-capillary hydraulic fall profile with $\tau = 0.7$, $F = 1.38$, past two obstructions characterised by $A_2 = 0.05$, $L_2 = 3.2$ and $A_1 = 0.02$, $L_1 = 3.2$ with $x_d = -20$. Initially, a steady free surface profile is utilized (the lowest profile in (a)). In (a) the vertical axis is then moved upwards by 0.01 for each plot shown, such that $t_n = 2n$ for plots $n = 0, ..., 7$. In (b) the solution profiles are this time viewed in a frame of reference moving with the obstructions. The solid line shows part of the solution at $t = 0$, and the dashed line part of the solution at $t = 14$.

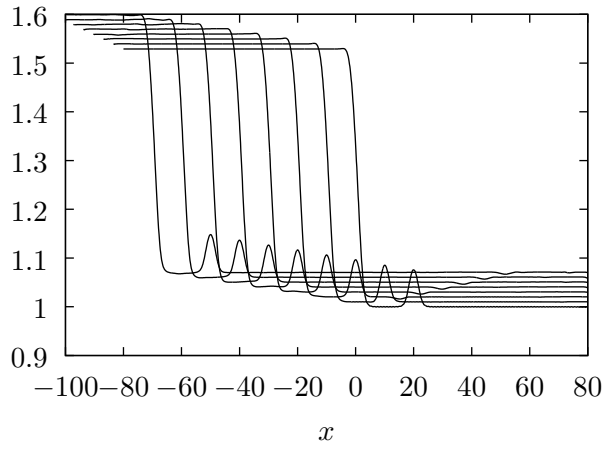

FIG. 11. Time evolution of a gravity-capillary hydraulic fall profile with $\tau = 0.3$, $F = 1.36$, past two obstructions characterised by $A_2 = 0.05$, $L_2 = 3.2$ and $A_1 = 0.02$, $L_1 = 3.2$ with $x_d = -20$. Initially, a steady free surface profile is utilized. The vertical axis is then moved upwards by 0.01 for each plot shown, such that $t_n = 10n$ for plots $n = 0, ..., 7$.

seen that the amplitude of the trapped waves has decreased with time, suggesting that the trapped waves between the two obstructions are unstable. However, the hydraulic fall over the first obstruction and the elevation wave over the second obstruction appear to be stable.

Page et al. showed that for weak surface tension, if the height of the downstream submerged obstruction is too small, any trapped waves that may exist between the obstructions, are not actually easily visible. In figure 11 we follow a typical solution profile, with $\tau = 0.3$, forward in time. This solution appears to be stable. Of course, we would expect that any trapped waves that do actually exist between the two obstructions, would still decay with time.

When the surface tension is very small, so that the upstream Froude number intersects the upstream linear dispersion relation, Page *et al.*[10] showed that gravity-capillary trapped waves could be obtained by placing the second obstruction upstream of the hydraulic fall. After obtaining such a steady solution, we use it as the initial profile in our numerical scheme, to advance the solution forward in time. Figure 12(a) shows typical solution profiles at different times. In figure 12(b) we show the initial solution at time $t = 0$ (the solid line), superimposed with the solution at time $t = 20$ (the dashed line). The amplitude of the trapped waves at time $t = 20$ is clearly smaller than the amplitude of those at $t = 0$. This suggests that this type of solution is unstable.

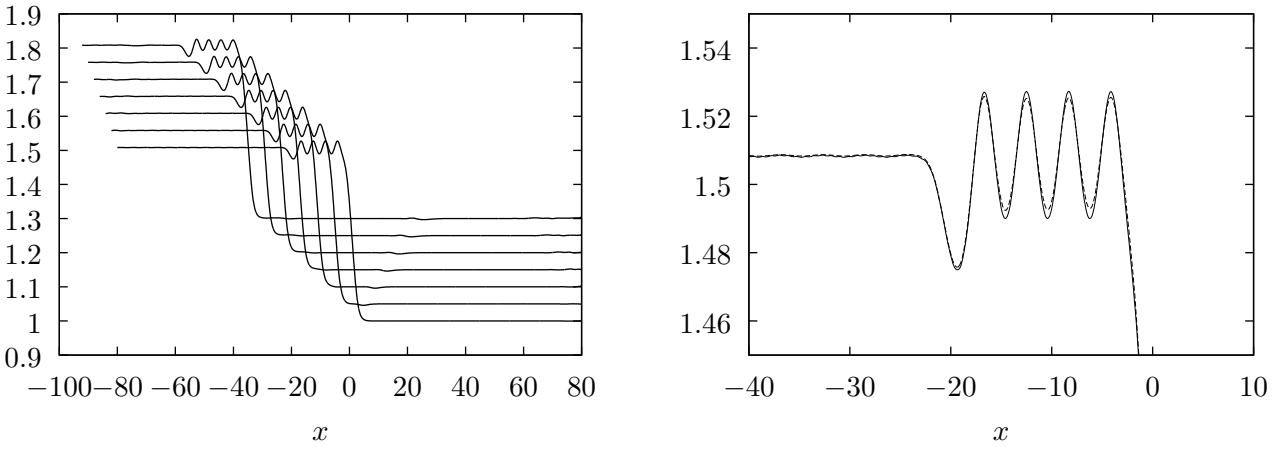

(a) (b)

FIG. 12. Time evolution of a gravity-capillary hydraulic fall profile with $\tau = 0.1$, $F = 1.35$, past two obstructions characterised by $A_2 = 0.05$, $L_2 = 3.2$ and $A_2 = 0.01$, $L_1 = 3.2$ with $x_d = 20$. Initially, a steady free surface profile is utilized (the lowest profile in (a)). In (a) the vertical axis is then moved upwards by 0.05 for each plot shown, such that $t_n = 6n$ for plots $n = 0, ..., 6$. In (b) the solution profiles are this time viewed in a frame of reference moving with the obstructions. The solid line shows part of the solution at $t = 0$, and the dashed line part of the solution at $t = 20$.

It therefore appears that gravity-capillary trapped wave solutions may be unstable. The amplitude of the waves, whether they occur upstream or downstream, appears to decrease with time.

F. Gravity-capillary hydraulic falls with a solitary type wave

Providing that the surface tension is not so small that the upstream Froude number intersects the upstream linear dispersion relation, solitary type waves can be obtained upstream of the hydraulic fall, over the additional obstruction (see Page *et al.*[10]). A depression wave is obtained over a positively orientated obstacle. In figure 13 we follow such a solution, with $\tau = 0.7$, forward in time. The depression wave is seen to move with its underlying obstacle, suggesting that this solution is stable.

When the surface tension is weak there exists a minimum in the upstream linear dispersion relation. If the Froude number is close to the minimum, the solitary type wave in the steady solution has small decaying oscillations in its tail. In figure 14 we follow such a solution,

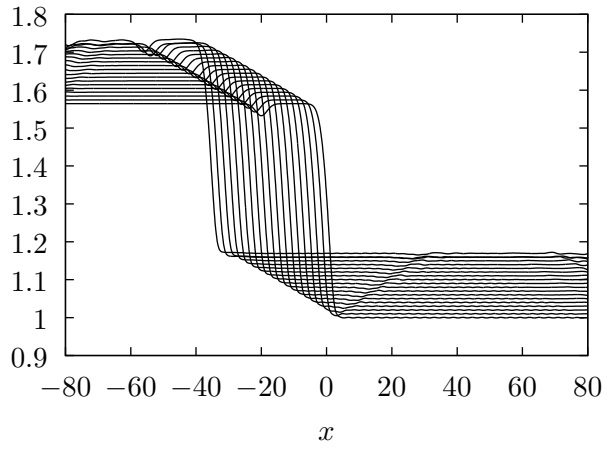

FIG. 13. Time evolution of gravity-capillary hydraulic fall profiles. Initially, a steady free surface profile over two obstructions is utilized. The second obstruction is placed upstream of the hydraulic fall. The vertical axis is then moved upwards by 0.01 for each plot shown, such that $t_n = 2n$ for plots $n = 0, ..., 16$.

found over a negatively orientated obstruction, forward in time. Figure 14(b) demonstrates how the solitary wave itself appears to maintain its shape as time evolves, but the decaying oscillations in the tail of the wave, appear to decreases in amplitude with time.

V. DISCUSSION

Unsteady, forced critical flow solutions were computed in both the pure gravity and gravity-capillary cases, for the fully nonlinear problem. By following the solutions in time, we assessed the stability of hydraulic falls past a single submerged obstruction, as well as the various results found in Dias and Vanden-Broeck[7], Belward[9] and Page *et al.*[10] for flow past two submerged obstructions.

It was shown that both the pure gravity and the gravity-capillary hydraulic falls are stable. This result, in the pure gravity case, is in agreement with the weakly nonlinear results obtained by Chardard *et al.*[11] and Donahue and Shen[12]. In the case of two submerged obstructions, it was shown that the solution with an upstream train of trapped waves between the two obstructions, are stable in the pure gravity case.

In the gravity-capillary case, both the solutions with trapped waves appearing downstream and the very small Bond number solutions with trapped waves appearing upstream,

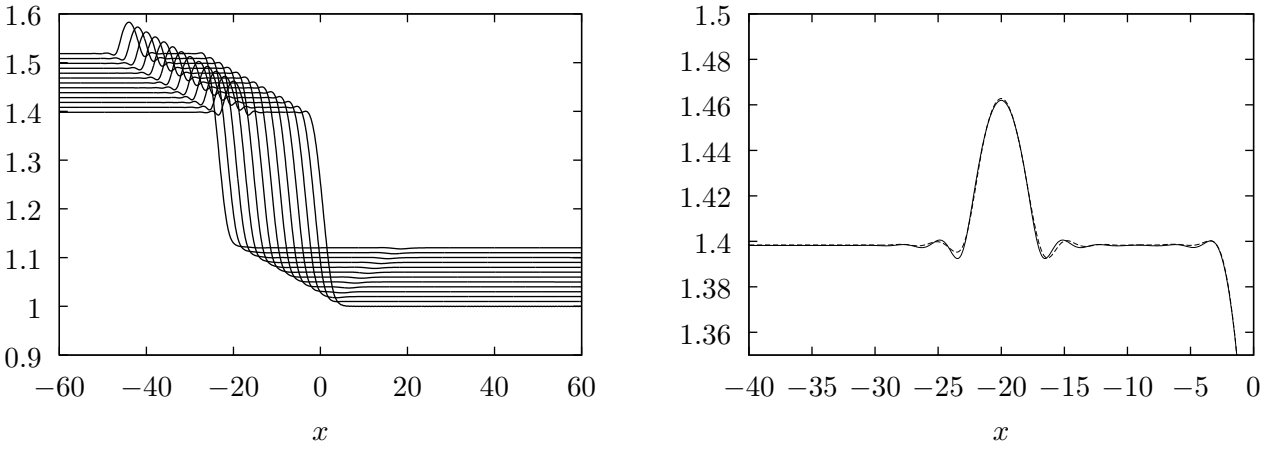

FIG. 14. Time evolution of a gravity-capillary hydraulic fall profile with $\tau = 0.19$, $F = 1.38$, past two obstructions characterised by $A_2 = 0.03$, $L_2 = 3.2$ and $A_1 = -0.03$, $L_1 = 3.2$ with $x_d = 20$. Initially, a steady free surface profile is utilized (the lowest profile in (a)). In (a) the vertical axis is then moved upwards by 0.01 for each plot shown, such that $t_n = 2n$ for plots $n = 0, ..., 12$. In (b) the solution profiles are this time viewed in a frame of reference moving with the obstructions. The solid line shows part of the solution at $t = 0$, and the dashed line part of the solution at $t = 19$.

appear to be unstable. We found that the amplitude of the waves decreases with time. In the absence of the current computational restraints, it may be of interest to follow these solutions further in time to see if the trapped waves between the submerged obstructions disappear completely. Furthermore, Page *et al.*[10] showed that there exist multiple families of gravity-capillary downstream trapped wave solutions. Here, we have considered the stability of only one of these types, but the stability of the other types may also be of interest.

When the free surface over the additional obstruction is a solitary type wave, we have shown that both the gravity and the gravity-capillary solutions appear to be stable. Of course, it should be noted that due to the computational limitations associated with solving such a fully nonlinear problem, we were only able to follow the free surface profiles so far in time. If we were able to advance the solutions much further in time, we may indeed discover that some of the 'stable' solutions presented in this paper do in fact later develop instabilities.

We have thus concluded that gravity and gravity-capillary hydraulic falls, gravity trapped

waves upstream of a hydraulic fall and hydraulic falls with a solitary type wave either upstream (in the gravity-capillary case) or downstream (in both the pure gravity and gravity-capillary cases) are stable. Three of these solutions, the pure gravity solutions, have been observed experimentally, for example, by Pratt[8]. We would therefore expect that all three of these solutions can be found naturally or in everyday situations, when the correct flow configurations present themselves. In the gravity-capillary case, one would therefore also expect to be able to observe/experiment with the hydraulic fall and the hydraulic fall superimposed with a solitary type wave further up or downstream. However, as we have ignored the effects of viscosity in our analysis, which very quickly dampens capillary waves, solutions where the surface tension is strong, are likely only to be observable at very shallow water depths. Furthermore, as we have concluded that gravity-capillary trapped waves up or downstream of a hydraulic fall are unstable, one would not expect such flows to be observed in nature.

We did not compute 'rising hydraulic falls' where the flow upstream of the hydraulic fall is supercritical and downstream is subcritical, so that the depth of the fluid increases over the submerged obstruction, due to the complexities in the boundary conditions. However, we speculate that such flows would be unstable. Pratt[8] considered the characteristic curves of solutions obtained using long-wave theory. He showed that in the case of two underlying obstructions where the flow was such that a hydraulic fall occured over the first obstruction and a 'rising hydraulic fall' occured over the second, or vice versa, the hydraulic fall was stable but the 'rising hydraulic fall' was not. Furthermore, 'rising fronts' are not observed in nature, see for example Viollet *et al.*[16]. This suggess that these flows are unstable.

ACKNOWLEDGMENTS

The research presented in this paper was carried out on the High Performance Computing Cluster supported by the Research and Specialist Computing Support service at the University of East Anglia. E.I.P. was supported by the EPSRC under grant EP/H008489/1. Both authors also wish to thank the anonymous referees for their helpful and constructive comments.

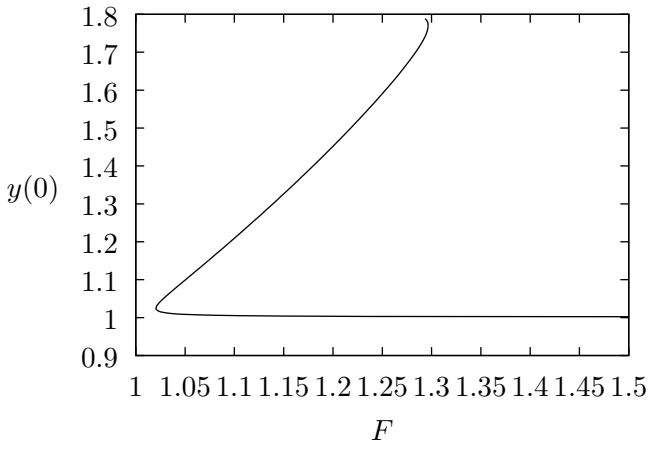

FIG. 15. Solitary wave solution branch. The underlying obstacle is characterised by $A_2 = 0.001$, $L_2 = 2$.

Appendix: Pure gravity solitary wave analysis

Steady forced solitary wave solutions are not unique. Vanden-Broeck[1] showed that for a particular range of Froude numbers there exist two solutions with the same value of F; a small amplitude wave bifurcating from the uniform stream and a large amplitude wave bifurcating from the pure solitary wave.

We consider pure gravity solutions over a single small obstacle, $A_2 = 0.001$, $L_2 = 2$. The steady forced solution branch in the $F - y(0)$ plane is well known, and is shown in figure 15. The lower part of the branch, before the turning point, corresponds to solutions bifurcating from the uniform stream. The upper part of the branch corresponds to forced solitary waves bifurcating from the pure solitary wave solution.

Firstly, we follow the initial steady solutions on the lower part of the branch, with $F = 1.1$, $F = 1.2$ and $F = 1.32$, forward in time. We find that the forced solitary wave is stable in each case. It moves upstream with the submerged obstruction. Solution profiles are shown in figure 16. Grimshaw and Maleewong[3] considered comparable solutions that were forced by a local pressure distribution. Our findings are in agreement with their results and thus confirm our solutions and methodology.

When the initial steady solution is on the upper part of the solution branch in figure 15, we find that the forced solitary wave is unstable. For F close to one we see that the forced solitary wave starts to move upstream away from the obstacle. For larger F the amplitude of

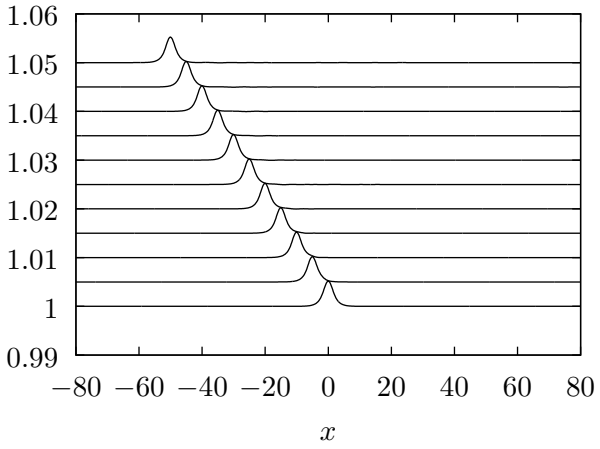

(a) F=1.10

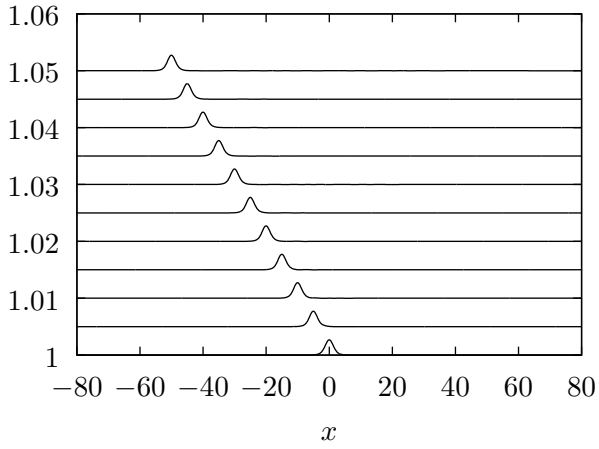

(b) F=1.32

FIG. 16. Evolution of pure gravity solitary waves with $F \approx 1.1$ and $F \approx 1.3$ in time. Initially, a steady solitary wave bifurcating from the uniform stream is utilized (the lowest profile). The vertical axis is then moved upwards by 0.005 for each plot shown, such that $t_n = 5n$ for plots $n = 0, ..., 10$.

the solitary wave sharpens very quickly, until the solution breaks at an early time. We show the evolution of the free surface in figure 17. Although it is hard to see in the figure, the solution profile at $t = 50$ in figure 17(a) has moved a distance of $x \approx 0.14$ upstream of the submerged obstruction. Again, our results are in agreement with work done by Grimshaw and Maleewong[3] for flow past a pressure distribution.

Next we add a small perturbation to the initial steady solution of the form

$$y = (1 - \alpha)y_0 + \alpha, \tag{A.1}$$

where $-0.1 \leq \alpha \leq 0.15$ and y_0 is the initial solution. We consider a larger obstacle than above and thus take $A_2 = 0.05$ and $L_2 = 3.2$.

When the steady solution bifurcating from the uniform stream is perturbed for any α, we find that the solitary wave recovers its original state and moves upstream with the obstruction, see figure 18. So again, we observe that this solitary wave is stable. Transient waves appear downstream of the solitary wave. This result is in agreement with the results of Chardard *et al.*[11], obtained using a fKdV equation.

The solution bifurcating from the pure solitary wave is again shown to be unstable. When the perturbation is less than the initial steady state solution, the amplitude of the solitary

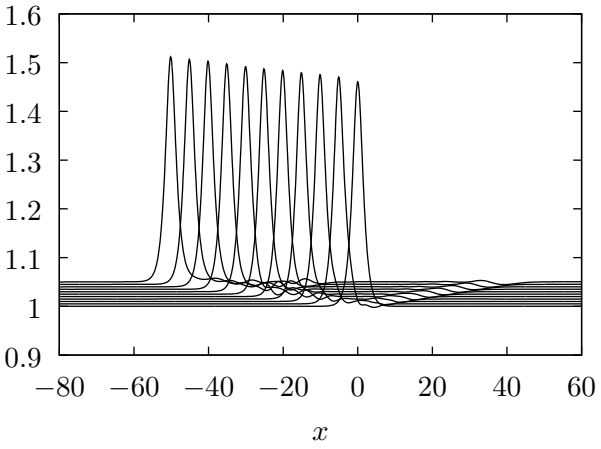

(a) F=1.20

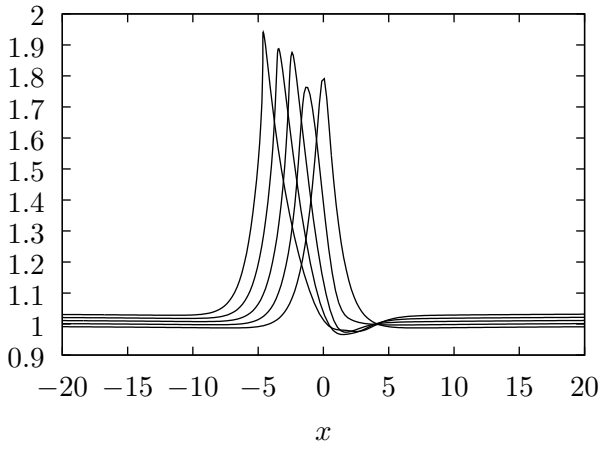

(b) F=1.29

FIG. 17. Evolution of pure gravity solitary waves with $F \approx 1.2$ and $F \approx 1.3$ in time. Initially, a steady solitary wave profile bifurcating from a pure solitary wave is utilized (the lowest profile). The vertical axis is then moved upwards by (a) 0.005 for each plot shown, such that $t_n = 5n$ for plots $n = 0, ..., 10.$, and (b) 0.01 for each plot shown, such that $t_n = n$ for plots $n = 0, ..., 4$.

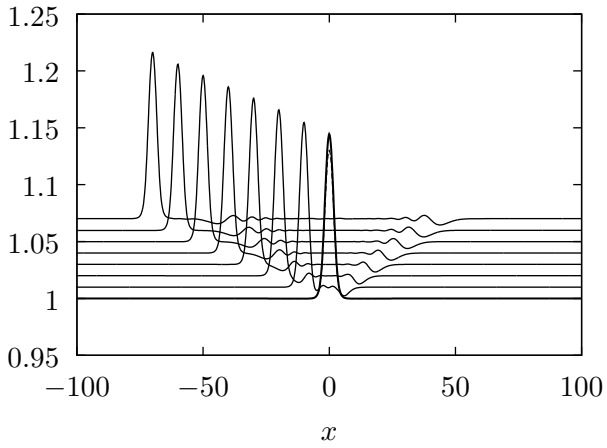

(a) F=1.5

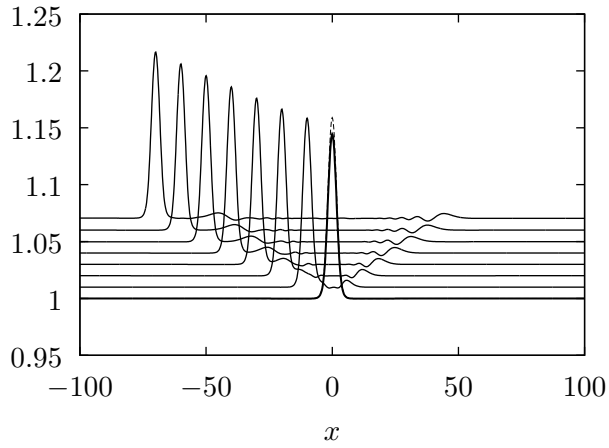

(b) F=1.5

FIG. 18. Evolution of pure gravity solitary waves with $F = 1.5$ in time. Initially, a steady solitary wave bifurcating from the uniform stream, perturbed by (A.1), is utilized. The bold solution shows the initial solitary wave. The dashed line is the perturbed solution when (a) $\alpha = 0.1$ and (b) $\alpha = -0.1$. The vertical axis is moved upwards by 0.01 for for each plot shown, such that $t_n = 10n$ for plots $n = 0, ..., 7$.

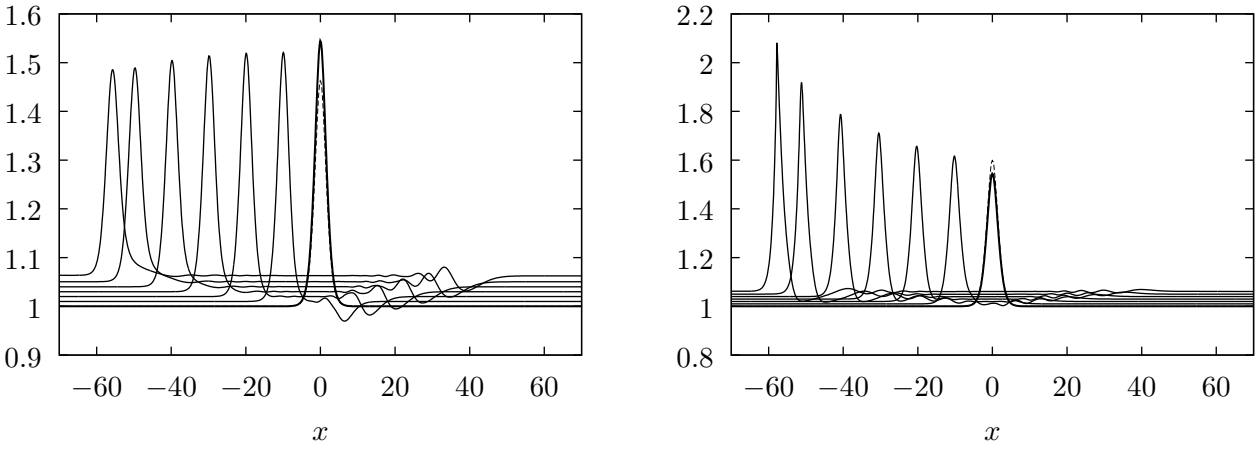

(a) F=1.3 (b) F=1.3

FIG. 19. Evolution of perturbed pure gravity solitary waves with $F = 1.3$ in time. Initially, a steady solitary wave bifurcating from a pure solitary wave, perturbed by (A.1), is utilized. The bold solution shows the initial solitary wave. The dashed line is the perturbed solution when (a) $\alpha = 0.15$ and (b) $\alpha = -0.1$.. The vertical axis is moved upwards by 0.01 for each plot shown, such that $t_n = 10n$ for plots $n = 0, ..., 5, 5.6$.

wave is found to decrease, see figure 19(a). When the perturbation is greater than the steady state solution we see that the amplitude of the solitary wave increases. The crest sharpens until eventually the wave breaks, see figure 19(b). In their weakly nonlinear analysis using a fKdV equation, Chardard *et al.*[11] obtained similar results. They found that with the smaller perturbation, the solitary wave decreases towards the stable bifurcation from the uniform stream. For the larger perturbation, their scheme was unable to predict breaking of the waves. Instead they found solutions where the large solitary wave propagated upstream away from the obstruction, leaving behind a solitary wave bifurcating from the uniform stream.

REFERENCES

[1]J.-M. Vanden-Broeck, "Free-surface flow over an obstruction in a channel," Phys. Fluids **30**, 2315 (1987).

[2]R. Grimshaw, M. Maleewong, and J. Asavanant, "Stability of gravity-capillary waves generated by a moving pressure disturbance in water of finite depth," Phys. Fluids **21**,

082101 (2009).

[3]R. Grimshaw and M. Maleewong, "Stability of steady gravity waves generated by a moving localised pressure disturbance in water of finite depth," Phys. Fluids **25**, 076605 (2013).

[4]S. Grandison and J.-M. Vanden-Broeck, "Truncation approximations for gravity-capillary free-surface flows," J. Eng. Math. **54**, 89 (2006).

[5]L. Forbes, "Critical free-surface flow over a semi-circular obstruction," J. Eng. Math **22**, 3 (1988).

[6]F. Dias and J. Vanden-Broeck, "Generalised critical free-surface flows," J. Eng. Math. **42**, 291 (2002).

[7]F. Dias and J.-M. Vanden-Broeck, "Trapped waves between submerged obstacles," Eur. J. Mech. - B/Fluids **509**, 93 (2004).

[8]L. J. Pratt, "On nonlinear flow with multiple obstructions," J. Atmospheric Sci. **41**, 1214 (1984).

[9]S. Belward, "Fully nonlinear flow over successive obstacles: hydraulic fall and supercritical flows," J. Aust. Math. Soc. Ser. B. **40**, 447 (1999).

[10]C. Page, S. Grandison, and E. Părău, "The influence of surface tension upon trapped waves and hydraulic falls," Eur. J. Mech. - B/Fluids **43**, 191 (2014).

[11]F. Chardard, F. Dias, H. Nguyen, and J.-M. Vanden-Broeck, "Stability of some stationary solutions to the forced kdv equation with one or two bumps," J. Eng. Math. **70**, 175 (2011).

[12]A. Donahue and S. Shen, "Stability of hydraulic fall and sub-critical cnoidal waves in water flows over a bump," J. Eng. Math. **68**, 197 (2010).

[13]M. Cooker, D. Peregrine, C. Vidal, and J. Dold, "The interaction between a solitary wave and a submerged semicircular cylinder," J. Fluid Mech. **215**, 1 (1990).

[14]J. Dold, "An efficient surface-integral algorithm applied to unsteady gravity waves," Journal of Computational Physics **103**, 90 (1992).

[15]F. Dias and J.-M. Vanden-Broeck, "Two-layer hydraulic falls over an obstacle," Eur. J. Mech. - B/Fluids **23**, 879 (2004).

[16]P.-L. Viollet, J.-P. Chabard, P. Esposito, and D. Laurence, *Mécanique des Fluides Appliquée.* (Presses de l'Ecole Nationale des Ponts et Chaussées., 1998).